Analysis of higher order composite beams by exact and finite element methods

Guang-hui He[*] and Xiao Yang

Department of Civil Engineering, Shanghai University, Shanghai, China

Abstract.   In this paper, a two-layer partial interaction composite beams model considering the higher order shear deformation of sub-elements is built. Then, the governing differential equations and boundary conditions for static analysis of linear elastic higher order composite beams are formulated by means of principle of minimum potential energy. Subsequently, analytical solutions for cantilever composite beams subjected to uniform load are presented by Laplace transform technique. As a comparison, FEM for this problem is also developed, and the results of the proposed FE program are in good agreement with the analytical ones which demonstrates the reliability of the presented exact and finite element methods. Finally, parametric studies are performed to investigate the influences of parameters including rigidity of shear connectors, ratio of shear modulus and slenderness ratio, on deflections of cantilever composite beams, internal forces and stresses. It is revealed that the interfacial slip has a major effect on the deflection, the distribution of internal forces and the stresses.

Keywords: composite beams; Timoshenko beam theory; higher order shear deformation; shear effect; laplace transform; finite element method

1. Introduction

Composite beams are extensively utilized in structural engineering, aerospace, automotive and underwater problems, as they make better use of material properties of their components. For instance, timber-concrete or steel-concrete elements are widely applied to civil engineering. Due to the stiffness of the shear connectors, which connect each sub-element as a whole, a variety of mathematical models have been proposed. Early works tended to neglect the effects of transverse shear deformation and interfacial shear slip between sub-elements, i.e., a full shear interaction can be achieved with a rigid connection. Recently, researchers (Schnabl *et al.* 2007a, b), however, have found that the shear deformation of sub-layers and the stiffness of the shear connectors influence significantly on the mechanical behavior of thick two-layer composite beams.

Based on the small deformation elastic hypothesis and the Euler-Bernoulli's beam theory (EBT), Newmark *et al.* (1951) initially introduced mathematical model for composite beams with partial interaction, which is still being widely used today and is further improved by many researchers. For example, Erkmen and Attard (2011) and Dall'Asta and Zona (2002), incorporated

---

∗Corresponding author, Ph.D. Student, E-mail: flamehe@shu.edu.cn

material nonlinearity and nonlinear connectors into Newmark's model; Kroflič *et al.* (2010) even took into account the uplift (deflection discrepancy of each sub-member), though they still conformed to Newmark's geometrically linear Euler-Bernoulli beam theory. Further, Ranzi *et al.* (2010), Battini *et al.* (2009) improved Newmark's model by considering the geometric nonlinearity, and presented corresponding FE formulations; Kroflič *et al.* (2011) derived FE formulations for a two-layer composite beams considering material nonlinearity as well as geometric nonlinearity. When it comes to the theoretical study, Newmark's governing differential equations have become the prototype again for improving, e.g., Faella *et al.* (2002) proposed exact FEM for static analysis, using the general solutions. Ouyang *et al.* (2012) built a mathematical model taking into account the large deflection of two-layer composite beams based on Newmark's model, and subsequently analytical solutions was provided for the case of linearly reduced.

Shear effects of composite beams tend to be significant, when their span-to-depth ratio gets smaller, as a result, Timoshenko composite beams may fit better. Ranzi and Zona (2007), Schnabl *et al.* (2007a, b), Nguyen *et al.* (2011), Grognec *et al.* (2012) modeled sub-elements of two-layer partial interaction composite beams with Timoshenko beams or Euler-Bernoulli coupling with Timoshenko beam, where the static and buckling problems are solved analytically or numerically. Furthermore, Hjiaj *et al.* (2012), Čas *et al.* (2004), Zona and Ranzi (2011) described each sub-element of composite beams with Timoshenko beam theory (TBT) taking into account the material or geometric nonlinearity, and static analysis was committed by FEM as well. Unfortunately, it's a tough problem (Whitney 1973) to obtain Timoshenko's shear correction factor for composite beams with partial interaction, due to the fact that the factor is attributed to each sub-element cross section's geometry as well as the shear stress around the section (Chakrabarti *et al*. 2012), unlike the case of single beam's cross section with free stress boundary. To overcome this drawback, it's an alternative to use higher order shear deformable beam theory. Hence, Chakrabarti *et al.* (2012) used Reddy's higher order beam theory (Reddy 1984), assuming that shear stresses over beam depth vary as quadratic polynomial and vanishes at the top and bottom of beam, as a result, the introduction of shear correction factor was avoided. Similarly, Li *et al*. (2013) assumed that shear stresses distributed along the beam depth hyperbolically. Vo and Thai (2012) used various of refined shear deformation theories in the static analysis for composite beams.

Obviously, FEM has become the mainstream engineers prefer to deal with composite beams problem, however, to the best knowledge of the authors, there's no literature on exact analytical solutions for higher order composite beams subjected to static load, which motivates us to do this study. In this study, we replace Euler-Bernoulli's hypothesis with Reddy's theory (Reddy 1984), as an improvement of Newmark's model. According to the principle of minimum potential energy, the governing differential equations and boundary conditions are formulated for composite beams subjected to uniform load, and the solutions are obtained by Laplace transform technique. More than that, a new finite element with 3 nodes and 18 degrees of freedom (dof) is derived. Compared with the work of Chakrabarti *et al.* (2012), who proposed a finite element with 3 nodes and 24 dofs, the present study optimizes the configuration of dofs of the finite element (Chakrabarti *et al*. 2012) and avoids the introduction of penalty factors (Cook *et al*. 2007) used by Chakrabarti *et al*. (2012), which may cause numerical problems (Cook *et al*. 2007). Two examples of two-layer composite beam structures, including a cantilever and a simply supported two-layer composite beams subjected to uniform load, are presented. The results indicate that exact solutions are in good agreement with those of FEM. Finally, parameters, including the interfacial slip stiffness, the ratio of shear modulus and the span-to-depth ratio, are studied in the parametric analysis.
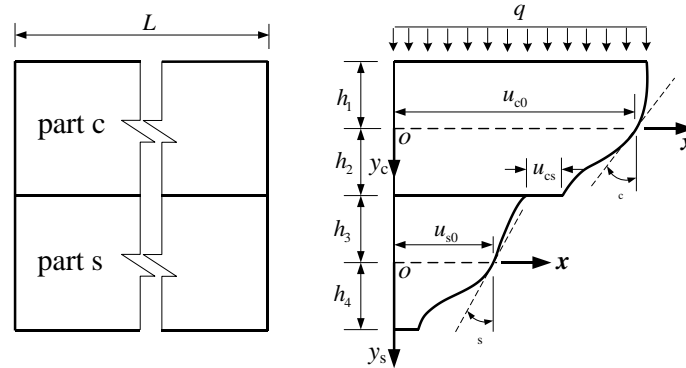
Fig. 1 Axial displacement fields of Reddy's composite beams

2. Formulation

Let us consider a two-layer composite beam (see Fig. 1), subjected to uniform load q on top of layer c, whose overall span is L, and they consist of upper layer c and lower layer s. Two coordinate systems are set up at the centroid of each layer at the left end, and geometric information is shown in Fig. 1, i.e., two centroid axes and the shear connectors divide the whole depth of composite beams into four sub-depths, which are h_1, h_2, h_3 and h_4. u_{c0} and u_{s0} denote axial displacements at centroid for part c and s respectively; u_{cs} means the interfacial slip between part c and s. Generalized rotation of upper section θ_c and lower section θ_s represent the tangent slope at the centroid of part c and s respectively.

For the completeness of the paper, herein the kinematics of two-layer composite beams is repeated (Yang and He 2014). According to Reddy's higher order beam hypothesis (Reddy 1984) on axial displacement of the 'fibers' over the beam depth for layer c and s can be expressed as

$$u_i(x, y_i) = u_{i0}(x) - \theta_i(x)y_i + \alpha_i(x)y_i^2 + \delta_i(x)y_i^3, \quad i = c, s \tag{1}$$

where u_i is the axial displacement of layer i; $\alpha_i(x)$ and $\delta_i(x)$ are the coefficients for higher order terms.

The interfacial slip can simply be formulated from the discrepancy between the axial displacement at the bottom surface of the upper layer and that at the top surface of the lower layer, thus

$$u_{cs}(x) = u_c(x, h_2) - u_s(x, -h_3) \tag{2}$$

Neglecting the vertical separation between layers, the transverse displacement for both layers can be expressed as

$$w_c(x) = w_s(x) = w(x) \tag{3}$$

Shearing strain γ_i and stress T_i over the cross section can be obtained according to the theory of elasticity, which assumes that the displacement and strain of structure are both small, thus we have

$$\gamma_i = \frac{\partial u_i}{\partial y_i} + \frac{\partial w}{\partial x} = -\theta_i + 2y_i\alpha_i + 3y_i^2\delta_i + w', \quad T_i = G_i\gamma_i \tag{4}$$

where G_i is the shear modulus of layer i (i=c, s), and hereafter the superscript '′' denotes the derivative with respect to x, i.e., $(\bullet)'=d(\bullet)/dx$.

Two stress boundary conditions can be obtained from free shearing stress conditions on the top of layer c or at the bottom of layer s, that is

$$T_c(-h_1) = 0, \quad T_s(h_4) = 0 \tag{5}$$

The other two conditions can be obtained from the interfacial shear flow. Assuming that shear flow of shear connectors uniformly smears over the interface, yields

$$T_c(h_2)b_c = k_{cs}u_{cs}, \quad T_s(-h_3)b_s = k_{cs}u_{cs} \tag{6}$$

where b_c is the bottom edge's width of section c; b_s is the top edge's width of section s; k_{cs} is the rigidity of shear connectors.

Higher order coefficients α_i and δ_i can be determined by Eqs. (5) and (6), and written as follows

$$[\alpha_c \quad \delta_c \quad \alpha_s \quad \delta_s] = [\mathbf{A}_1\mathbf{e} \quad \mathbf{A}_2\mathbf{e} \quad \mathbf{A}_3\mathbf{e} \quad \mathbf{A}_4\mathbf{e}] \tag{7}$$

where

$$\mathbf{e}=[u_{c0} \quad \theta \mathrm{c} \quad u_{s0} \quad \theta_s \quad w']^{\mathrm{T}} \tag{8}$$

Matrix $\mathbf{A}$ is composed of four row vectors $\mathbf{A}_1$, $\mathbf{A}_2$, $\mathbf{A}_3$ and $\mathbf{A}_4$, that is

$$\mathbf{A} = [\mathbf{A}_1^T \quad \mathbf{A}_2^T \quad \mathbf{A}_3^T \quad \mathbf{A}_4^T] \tag{9}$$

in which, $\mathbf{A} = \mathbf{S}_1^{-1}\mathbf{S}_2$; $\mathbf{S}_1$ and $\mathbf{S}_2$ have following expressions

$$S_1 = \begin{bmatrix} 2G_ch_1 & 3G_ch_1^2 & 0 & 0 \\ 0 & 0 & -2G_sh_4 & 3G_sh_4^2 \\ -\dfrac{h_2(2b_cG_c + h_2k_{cs})}{b_c} & h_2^2\left(3G_c + \dfrac{h_2k_{cs}}{b_c}\right) & \dfrac{h_3^2k_{cs}}{b_c} & \dfrac{h_3^3k_{cs}}{b_c} \\ -\dfrac{h_2^2k_{cs}}{b_s} & \dfrac{h_2^3k_{cs}}{b_s} & h_3\left(2G_s + \dfrac{h_3k_{cs}}{b_s}\right) & h_3^2\left(3G_s + \dfrac{h_3k_{cs}}{b_s}\right) \end{bmatrix} \tag{10}$$

$$S_2 = \begin{bmatrix} 0 & G_c & 0 & 0 & -G_c \\ 0 & 0 & 0 & G_s & -G_s \\ \dfrac{k_{cs}}{b_c} & G_c + \dfrac{h_2k_{cs}}{b_c} & -\dfrac{k_{cs}}{b_c} & \dfrac{h_3k_{cs}}{b_c} & -G_c \\ \dfrac{k_{cs}}{b_s} & \dfrac{h_2k_{cs}}{b_s} & -\dfrac{k_{cs}}{b_s} & G_s + \dfrac{h_3k_{cs}}{b_s} & -G_s \end{bmatrix} \tag{11}$$

Thus, higher order terms of axial displacement are eliminated by substituting Eq. (7) into Eq. (1), and an eliminated form of axial displacement are derived as

$$u_c = \mathbf{me}, \quad u_s = \mathbf{ne} \tag{12}$$

where row vectors $\mathbf{m}=\lambda_c+y_c^2\mathbf{A}_1+y_c^3\mathbf{A}_2$, $\mathbf{n}=\lambda_s+y_s^2\mathbf{A}_3+y_s^3\mathbf{A}_4$, $\lambda_c=[1 \quad -y_c \quad 0 \quad 0 \quad 0]$ and $\lambda_s=[0 \quad 0 \quad 1 \quad -y_s \quad 0]$.

With the help of Eq. (12) and small strain assumption of structure, normal strains of each layer over the cross section can be formulated as

$$\varepsilon_c = \frac{\partial u_c}{\partial x} = \mathbf{m}\mathbf{e}', \quad \varepsilon_s = \frac{\partial u_s}{\partial x} = \mathbf{n}\mathbf{e}' \tag{13}$$

The cross-sectional normal stresses of isotropic linear elastic layers can be obtained as

$$\sigma_c = E_c\mathbf{m}\mathbf{e}', \quad \sigma_s = E_s\mathbf{n}\mathbf{e}' \tag{14}$$

For the simplicity of notation of the following formulation, a strain vector storing the normal and shearing strains of each layer is introduced as

$$\boldsymbol{\varepsilon}_i = \mathbf{T}_i\begin{bmatrix} \mathbf{e}'^T & \mathbf{e}^T \end{bmatrix}^T, \quad i = c, s \tag{15}$$

where $\boldsymbol{\varepsilon}_i$ is a vector composed of normal strain ε_i and shear strain γ_i at cross section, that is, $\boldsymbol{\varepsilon}_i = [\varepsilon_i\ \gamma_i]^T$; matrices $\mathbf{T}_c$ and $\mathbf{T}_s$ can be constructed as

$$\mathbf{T}_c = \begin{bmatrix} \mathbf{m} & \mathbf{0} \\ \mathbf{0} & \dfrac{d\mathbf{m}}{dy_c} \end{bmatrix} + \boldsymbol{\Xi}, \quad \mathbf{T}_s = \begin{bmatrix} \mathbf{n} & \mathbf{0} \\ \mathbf{0} & \dfrac{d\mathbf{n}}{dy_c} \end{bmatrix} + \boldsymbol{\Xi} \tag{16}$$

in which, $\boldsymbol{\Xi} = [0\ \ 0\ \ 0\ \ 0\ \ 1]$. Using Eqs. (4) and (14), a matrix form of isotropic linear elastic constitutive can be derived as

$$\boldsymbol{\sigma}_i = \mathbf{D}_i\,\boldsymbol{\varepsilon}_i \tag{17}$$

where $\boldsymbol{\sigma}_i$ is stress vector for layer i ($i=c, s$), composed of normal stress σ_i and shear stress T_i, i.e., $\boldsymbol{\sigma}_i = [\sigma_i\ \ T_i]^T$; $\mathbf{D}_i$ is elastic parameters matrix with expression

$$\mathbf{D}_i = \begin{bmatrix} E_i & 0 \\ 0 & G_i \end{bmatrix} \tag{18}$$

Substituting Eq. (15) into Eq. (17), yields

$$\boldsymbol{\sigma}_i = \mathbf{D}_i\mathbf{T}_i[\mathbf{e}'^T\ \ \mathbf{e}^T]^T \tag{19}$$

Using Eq. (15) and Eq. (19), the strain energy of the two layers can be expanded as

$$E_\varepsilon = \frac{1}{2}\iiint_V (\boldsymbol{\varepsilon}_e^T\boldsymbol{\sigma}_c + \boldsymbol{\varepsilon}_s^T\boldsymbol{\sigma}_s)dAdx = \frac{1}{2}\int_0^L \begin{bmatrix} \mathbf{e}'^T & \mathbf{e}^T \end{bmatrix}\mathbf{D}\begin{bmatrix} \mathbf{e}'^T\mathbf{e}^T \end{bmatrix}^T dx \tag{20}$$

where

$$\mathbf{D} = \iint_{A_c} \mathbf{T}_c^T\mathbf{D}_c\mathbf{T}_c dA_c + \iint_{A_x} \mathbf{T}_s^T\mathbf{D}_s\mathbf{T}_s dA_s \tag{21}$$

and A_i ($i=c, s$) is the integral domain of layer i.

After simplifying Eq. (21), $\mathbf{D}$ can be blocked into a form of

$$\mathbf{D} = \begin{bmatrix} \mathbf{D}_{11} & 0 \\ 0 & \mathbf{D}_{22} \end{bmatrix} \tag{22}$$

where $\mathbf{D}_{11}$ and $\mathbf{D}_{22}$ are matrices of dimensions 5 by 5, and $\mathbf{0}$ denotes zero matrix of dimensions 5 by 5.

E_{cs} is the strain energy of the shear connectors at the interface, which can be written as

$$E_{cs} = \frac{1}{2}\int_0^L k_{cs}u_{cs}{}^2 dx \qquad (23)$$

where u_{cs} can be expressed by Eqs. (24) and (25)

$$u_{cs} = \mathbf{b}\mathbf{e} \qquad (24)$$

and

$$\mathbf{b} = \mathbf{m}\Big|_{y_c=h_2} - \mathbf{n}\Big|_{y_s=-h_4} \qquad (25)$$

The work done by the external force herein is indicated by W_{ex}. In the case of a uniform transversely distributed pressure q (see Fig. 1) acting on the upper surface of the composite beams, we have

$$W_{cx} = \int_0^L qw dx \qquad (26)$$

Subsequently, the total potential energy $\prod$ is obtained with respect to u_{c0}, u_{s0}, θ_c, θ_s and w.

$$\prod[u_{c0}, u_{s0}, \theta_c, \theta_s, w] = E_\varepsilon + E_{cs} - W_{ex} \qquad (27)$$

Principle of minimum potential energy can be expressed as $\delta\prod=0$, by which the following set of differential equations is obtained

$$\mathbf{V}_{i1}\mathbf{e} + \mathbf{V}_{i2}\mathbf{e}'' = 0, \quad i = 1,2,3,4 \qquad (28)$$

$$\mathbf{V}_{51}\mathbf{e}' + \mathbf{V}_{52}\mathbf{e}''' = q \qquad (29)$$

where coefficient vectors $\mathbf{V}_{i1}$ and $\mathbf{V}_{i2}$ have definitions as

$$\begin{bmatrix} \mathbf{V}_{i1} \\ \mathbf{V}_{i2} \end{bmatrix} = \begin{bmatrix} k_{cs}b_i\mathbf{b} + \mathbf{D}_{22}^i \\ -\mathbf{D}_{11}^i \end{bmatrix} \qquad (30)$$

in which b_i is the ith component of vector $\mathbf{b}$; $\mathbf{D}_{11}^i$ is a vector composed of the ith row of $\mathbf{D}_{11}$.

Boundary conditions can also be derived as

$$\left[\mathbf{D}_{11}^i\mathbf{e}'\delta\mathbf{e}_i\right]_0^L = 0, \quad i = 1,2,3,4,5 \qquad (31)$$

$$\left[(\mathbf{V}_{51}\mathbf{e} + \mathbf{V}_{52}\mathbf{e}'')\delta w\right]_0^L = 0 \qquad (32)$$

where $\mathbf{e}_i\,(i = 1, 2, \ldots, 5)$ denotes the ith component of vector $\mathbf{e}$.

3. Exact method

Eqs. (28)-(29) compose a differential algebraic system, which can be transformed into a system

(a) clamped-free boundary conditions   (b) cross section of the composite beams
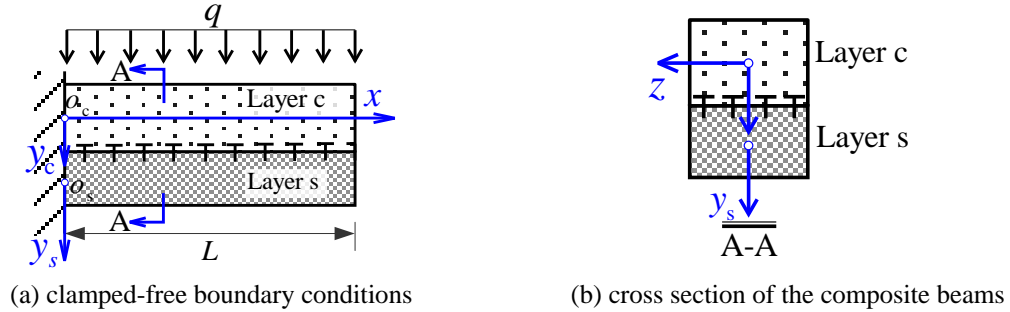
Fig. 2 A two-layer composite beams subjected to the uniform distributed pressure with (a) clamped-free boundary conditions and (b) their cross section

of ODEs. A matrix form of ODE system can be formulated below by virtue of Eq. (28)

$$\mathbf{A}_0\begin{bmatrix} u_{c0} & \theta_c & u_{s0} & \theta_s & w' \end{bmatrix}^T + \mathbf{B}_1\begin{bmatrix} u''_{c0} & \theta''_c & u''_{s0} & \theta''_s \end{bmatrix}^T + \boldsymbol{\alpha}w''' = \mathbf{0} \tag{33}$$

where coefficient matrices $\mathbf{A}_0$ and $\mathbf{B}_1$ are defined as

$$\mathbf{A}_0 = \begin{bmatrix} \mathbf{V}_{11}^T & \mathbf{V}_{21}^T & \mathbf{V}_{31}^T & \mathbf{V}_{41}^T \end{bmatrix}^T, \quad B_0 = \begin{bmatrix} \mathbf{V}_{12}^T & \mathbf{V}_{22}^T & \mathbf{V}_{32}^T & \mathbf{V}_{42}^T \end{bmatrix}^T \equiv \begin{bmatrix} \mathbf{B}_1 & \boldsymbol{\alpha} \end{bmatrix} \tag{34}$$

in which $\mathbf{B}_1$ is a block of matrix $\mathbf{B}_0$ with dimensions of 4 by 4; $\boldsymbol{\alpha}$ is the rest column of $\mathbf{B}_0$.

By solving the system of Eq. (33), the second order derivative terms can be obtained as

$$\begin{bmatrix} u''_{c0} & \theta''_c & u''_{s0} & \theta''_s \end{bmatrix}^T = -\mathbf{B}_1^{-1}\left(\boldsymbol{\alpha}w''' + \mathbf{A}_0\begin{bmatrix} u_{c0} & \theta_c & u_{s0} & \theta_s & w'' \end{bmatrix}^T\right) \tag{35}$$

A cantilever composed of composite beams (see Fig. 2), which is subjected to uniform transverse load q, is to be studied by the proposed Laplace transform technique.

The Laplace transform technique is a helpful mathematical tool for ordinary differential equations solving, and this transform has definition

$$\bar{f}(s) = \int_0^{+\infty} f(x)e^{-sx}dx \tag{36}$$

which describes that function in real domain $f(x)$ is transformed into complex domain $\bar{f}(s)$. Hereafter superscript short dash denotes function in Laplace domain. Conversely, the inverse Laplace transform is defined as

$$f(x) \equiv L_s^{-1}\left[\bar{f}(s)\right] = \frac{1}{2\pi i}\int_{a-i\infty}^{a+i\infty} \bar{f}(s)e^{sx}ds \tag{37}$$

According to the cantilever boundary conditions (see Fig. 2), we have

$$\mathbf{e}\big|_{x=0} = \mathbf{0}, \quad w\big|_{x=0} = 0 \tag{38}$$

By Laplace transform (36) and boundary conditions (38), governing differential equations (28) can be transformed into

$$\mathbf{A}_0 \begin{bmatrix} \bar{u}_{c0} \\ \bar{\theta}_c \\ \bar{u}_{s0} \\ \bar{\theta}_s \\ s\bar{w} \end{bmatrix} + \mathbf{B}_0 \begin{bmatrix} s^2\bar{u}_{c0} - c_1 \\ s^2\bar{\theta}_c - c_2 \\ s^2\bar{u}_{s0} - c_3 \\ s^2\bar{\theta}_s - c_4 \\ s^2\bar{w} - c_5 \end{bmatrix} = \begin{bmatrix} 0 \\ 0 \\ 0 \\ 0 \\ 0 \end{bmatrix} \tag{39}$$

where

$$[c_1 \quad c_2 \quad c_3 \quad c_4 \quad c_5 \quad c_6] = [u'_{c0} \quad \theta'_c \quad u'_{s0} \quad \theta'_s \quad w'' \quad w''']_{x=0} \tag{40}$$

Applying boundary conditions (38) to Eq. (35), it reduces to

$$[u''_{c0} \quad \theta''_c \quad u''_{s0} \quad \theta''_s]^T \big|_{x=0} = -\mathbf{B}_1^{-1}\boldsymbol{\alpha}w''' \big|_{x=0} \equiv [g_1 \quad g_2 \quad g_3 \quad g_4]^T c_6 \tag{41}$$

With the help of Eq. (38) and (41), Eq. (29) can be transformed into Eq. (42) by Eq. (36)

$$\mathbf{V}_{51} \begin{bmatrix} s\bar{u}_{c0} \\ s\bar{\theta}_c \\ s\bar{u}_{s0} \\ s\bar{\theta}_s \\ s^2\bar{w} \end{bmatrix} + \mathbf{V}_{52} \begin{bmatrix} s^3\bar{u}_{c0} - sc_1 - g_1 c_6 \\ s^3\bar{\theta}_c - sc_2 - g_2 c_6 \\ s^3\bar{u}_{s0} - sc_3 - g_3 c_6 \\ s^3\bar{u}_s - sc_4 - g_4 c_6 \\ s^4\bar{w} - sc_5 - c_6 \end{bmatrix} = \frac{q}{s} \tag{42}$$

Straightforward, Eq. (39) can be rewritten as

$$\left(\mathbf{A}_0 + s^2\mathbf{B}_0\right)[\bar{u}_{c0} \quad \bar{\theta}_{c0} \quad \bar{u}_{s0} \quad \bar{\theta}_c \quad s\bar{w}]^T = \mathbf{B}_0\mathbf{T}_1\mathbf{C} \tag{43}$$

where $C=[c^1 \quad c^2 \quad c^3 \quad c^4 \quad c^5 \quad c_6]^T$, and

$$\mathbf{T}_1 = \begin{bmatrix} \mathbf{I} & \mathbf{0} \\ \mathbf{0} & \Omega \end{bmatrix} \tag{44}$$

in which $\mathbf{I}$ is a 4th order identity matrix, and $\Omega=[1 \quad 0]$.

Thus, Eq. (42) can be rewritten as

$$\left(s\mathbf{V}_{51} + s^3\mathbf{V}_{52}\right)[\bar{u}_{c0} \quad \bar{\theta}_{c0} \quad \bar{u}_{s0} \quad \bar{\theta}_s \quad s\bar{w}]^T = \mathbf{V}_{52}(s\mathbf{T}_1 + \mathbf{T}_2)\mathbf{C} + q/s \tag{45}$$

where $\mathbf{T}_2 = [g_1 \quad g_2 \quad g_3 \quad g_4 \quad 1]^T [0 \quad 0 \quad 0 \quad 0 \quad 1]$.

Combining Eqs. (43) and (45), we have equation

$$[\bar{u}_{c0} \quad \bar{\theta}_{c0} \quad \bar{u}_{s0} \quad \bar{\theta}_s \quad s\bar{w}] = \mathbf{K}_1^{-1}\mathbf{K}_2\mathbf{C} + \mathbf{K}_1^{-1}\mathbf{R}$$
$$= [\mathbf{Q}_1^T \quad \mathbf{Q}_2^T \quad \mathbf{Q}_3^T \quad \mathbf{Q}_4^T \quad \mathbf{Q}_5^T]^T\mathbf{C} + [\rho_1 \quad \rho_2 \quad \rho_3 \quad \rho_4 \quad \rho_5]^T \tag{46}$$

where

$$\mathbf{K}_1 = \begin{bmatrix} \mathbf{A}_0 + s^2\mathbf{B}_0 \\ s\mathbf{V}_{51} + s^3\mathbf{V}_{52} \end{bmatrix}, \quad \mathbf{K}_2 = \begin{bmatrix} \mathbf{B}_0\mathbf{T}_1 \\ \mathbf{V}_{52}(s\mathbf{T}_1 + \mathbf{T}_2) \end{bmatrix} \tag{47}$$

$$\mathbf{K}_1^{-1}\mathbf{R} = [\rho_1 \quad \rho_2 \quad \rho_3 \quad \rho_4 \quad \rho_5]^T, \quad \mathbf{K}_1^{-1}\mathbf{K}_2 = [\mathbf{Q}_1^T \quad \mathbf{Q}_2^T \quad \mathbf{Q}_3^T \quad \mathbf{Q}_4^T \quad \mathbf{Q}_5^T]^T \qquad (48)$$

and

$$\mathbf{R} = [0 \quad 0 \quad 0 \quad 0 \quad 0 \quad q/s]^T \qquad (49)$$

By inverse Laplace transform, Eq. (46) can be inversed into the following set of equations

$$[u_{c0} \quad \theta_c \quad u_{s0} \quad \theta_s \quad w] = [\mathbf{\Phi}_1 C + r_1 \quad \mathbf{\Phi}_2 C + r_2 \quad \mathbf{\Phi}_3 C + r_3 \quad \mathbf{\Phi}_4 C + r_4 \quad \mathbf{\Phi}_5 C + r_5] \qquad (50)$$

where $L_s^{-1}(\rho_l) = r_l$, $L_s^{-1}(\mathbf{Q}_l) = \mathbf{\Phi}_l, l = 1, 2, 3, 4.$, $L_s^{-1}(\rho_5 / s) = r_5$ and $L_s^{-1}(\mathbf{Q}_5 / s) = \mathbf{\Phi}_5$.

The coefficient vector $\mathbf{C}$ can be determined from six boundary conditions at $x=L$, where u_{c0}, θ_c, u_{s0}, θ_s, w and w' are free. There are five boundary conditions from Eq. (31) can be expressed in terms of vector $\mathbf{C}$ as

$$\mathbf{K}_3 \mathbf{C} = \mathbf{\Gamma}_1 \qquad (51)$$

where $\mathbf{K}_3 = \mathbf{D}_{11}[\mathbf{\Phi}_1'^T \quad \mathbf{\Phi}_2'^T \quad \mathbf{\Phi}_3'^T \quad \mathbf{\Phi}_4'^T \quad \mathbf{\Phi}_5''^T]^T$ and $\mathbf{\Gamma}_1 = -\mathbf{D}_{11}[r_1' \quad r_2' \quad r_3' \quad r_4' \quad r_5'']$.

Similarly, by Eqs. (32) and (50), the sixth boundary condition is determined as

$$\mathbf{K}_4 \mathbf{C} = \mathbf{\Gamma}_2 \qquad (52)$$

where

$$\mathbf{K}_4 = \mathbf{V}_{51}[\mathbf{\Phi}_1^T \quad \mathbf{\Phi}_2^T \quad \mathbf{\Phi}_3^T \quad \mathbf{\Phi}_4^T \quad \mathbf{\Phi}' +_5^T]^T + \mathbf{V}_{52}[\mathbf{\Phi}_1''^T \quad \mathbf{\Phi}_2''^T \quad \mathbf{\Phi}_3''^T \quad \mathbf{\Phi}_4''^T \quad \mathbf{\Phi}_5'''^T]^T \qquad (53)$$

and

$$\mathbf{\Gamma}_2 = -\mathbf{V}_{51}[r_1 \quad r_2 \quad r_3 \quad r_4 \quad r_5']^T - \mathbf{V}_{52}[r_1'' \quad r_2'' \quad r_3'' \quad r_4'' \quad r_5''']^T \qquad (54)$$

By merging Eqs. (51) and (52), $\mathbf{C}$ can be solved as

$$\mathbf{C} = \begin{bmatrix} \mathbf{K}_3 \\ \mathbf{K}_4 \end{bmatrix}^{-1} \begin{bmatrix} \mathbf{\Gamma}_1 \\ \mathbf{\Gamma}_2 \end{bmatrix}, \quad x = L \qquad (55)$$

Consequently, the exact analytical solutions are obtained as Eq. (50) and (55). Although the above formulation is based on the clamped-free boundary conditions of the composite beams, the present solving method is general and can be applied to composite beams with arbitrary combinations of boundary conditions. When analyzing composite beams with other boundary conditions, due to the boundary conditions derived by variational principle (see Eq. (31) and (32)), there are always six boundary conditions can be obtained at $x=0$, and the other six boundary conditions at the point $x=L$.

4. Finite element method

Eq. (27) indicates that w has the highest derivative order of two, and that of the rest basic unknowns is one. In order to make sure that all the elements in vector $\mathbf{e}$ has interpolation order at least two, a finite element of length L (see Fig. 3) with three nodes is formulated, using Lagrange mixed with Hermite interpolation bases.
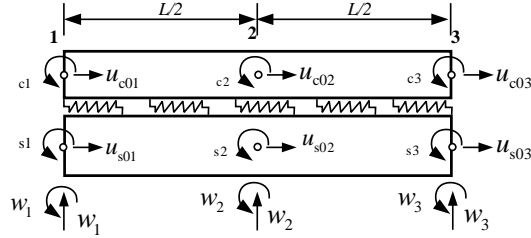
Fig. 3 Finite element of higher-order shear deformable composite beams

For u_{c0}, θ_c, u_{s0} and θ_s, Lagrange bases of node $x=0$, $L/2$ and L are constructed as

$$N_1 = \frac{(L-2x)(L-x)}{L^2}, \quad N_2 = \frac{4(L-x)x}{L^2}, \quad N_3 = \frac{(2x-L)x}{L^2} \tag{56}$$

$$u_{c0} \approx \sum_{k=1}^{3} N_k u_{c0k}, \quad u_{s0} \approx \sum_{k=1}^{3} N_k u_{s0k}, \quad \theta_c \approx \sum_{i=1}^{3} N_k \theta_{ck}, \quad \theta_s \approx \sum_{i=1}^{3} N_k \theta_{sk} \tag{57}$$

where u_{c0i}, u_{s0i}, θ_{ci} and θ_{si} denote the value of u_{c0}, u_{s0}, θ_c and θ_s at node i (see Fig. 3).

For w and w', Hermite bases are formulated as

$$\begin{cases} H_1 = \dfrac{(L-2x)^2(L-x)^2(L+6x)}{L^5}, & H_2 = \dfrac{x(x-L)^2(2x-L)^2}{L^4}, & H_3 = \dfrac{16(L-x)^2 x^2}{L^4}, \\ H_4 = \dfrac{8(2x-L)(L-x)^2 x^2}{L^4}, & H_5 = \dfrac{(7L-6x)(L-2x)^2 x^2}{L^5}, & H_6 = \dfrac{(L-2x)^2(x-L)x^2}{L^4} \end{cases} \tag{58}$$

$$w \approx \sum_{k=1}^{3} H_{2k-1} w_k + \sum_{k=1}^{3} H_{2k} w'_k, \quad w' \approx \sum_{k=1}^{3} H'_{2k-1} w_k + \sum_{k=1}^{3} H'_{2k} w'_k \tag{59}$$

where w_k and w'_k ($k=1, 2, 3$) are the nodal values of w and w' respectively, as is shown in Fig. 3.

Thus, a higher order finite element with three nodes is derived. And the vector of dofs for the entire element is defined as

$$\boldsymbol{\delta}_e = [\boldsymbol{\Psi}_1 \quad \boldsymbol{\Psi}_2 \quad \boldsymbol{\Psi}_3]^T \tag{60}$$

in which the nodal dof vector is

With the help of Eq. (57) and (59), the basic unknowns can be approximated as

$$u_{c0} \approx \mathbf{N}_{uc0} \boldsymbol{\delta_e}, \quad \theta_c \approx \mathbf{N}_{\theta c} \boldsymbol{\delta_e}, \quad u_{s0} \approx \mathbf{N}_{us0} \boldsymbol{\delta_e}, \quad \theta_s \approx \mathbf{N}_{\theta s} \boldsymbol{\delta_e}, \quad w \approx \mathbf{N}_w \boldsymbol{\delta_e} \tag{61}$$

where $\mathbf{N}_{uc0}$, $\mathbf{N}_{\theta c}$, $\mathbf{N}_{us0}$, $\mathbf{N}_{\theta s}$ and $\mathbf{N}_w$ denote row vectors of shape functions.

Using Eq. (61), the total potential energy of the structure formulated in Eq. (27) can be written as

$$\Pi = \frac{1}{2}\int_0^L \boldsymbol{\delta}_e^T \mathbf{N}_\varepsilon^T \mathbf{D} \mathbf{N}_\varepsilon \boldsymbol{\delta}_e dx + \frac{1}{2}\int_0^L k_{cs} \boldsymbol{\delta}_e^T \mathbf{N}_{cs}^T \mathbf{N}_{cs} \boldsymbol{\delta}_e dx - \int_0^L \mathbf{N}_w^T q \boldsymbol{\delta}_e dx \tag{62}$$

where

$$\mathbf{N}_{\varepsilon} = \begin{bmatrix} \mathbf{N}_{uc0}'^{T} & \mathbf{N}_{\theta 0}'^{T} & \mathbf{N}_{us0}'^{T} & \mathbf{N}_{\theta s}'^{T} & \mathbf{N}_{w}''^{T} & \mathbf{N}_{uc0}^{T} & \mathbf{N}_{\theta c}^{T} & \mathbf{N}_{us0}^{T} & \mathbf{N}_{\theta s}^{T} & \mathbf{N}_{w}'^{T} \end{bmatrix}^{T} \tag{63}$$

$$\mathbf{N}_{cs} = \mathbf{b} \begin{bmatrix} \mathbf{N}_{uc0}^{T} & \mathbf{N}_{\theta 0}^{T} & \mathbf{N}_{us0}^{T} & \mathbf{N}_{\theta s}^{T} & \mathbf{N}_{w}'^{T} \end{bmatrix}^{T} \tag{64}$$

According to the principle of minimum potential energy, we have

$$\frac{\partial \Pi}{\partial \delta_{e}} = \int_{0}^{L} \mathbf{N}_{\varepsilon}^{T} \mathbf{D} \mathbf{N}_{\varepsilon} dx \delta_{e} + \int_{0}^{L} k_{cs} \mathbf{N}_{cs}^{T} \mathbf{N}_{cs} dx \delta_{e} - \int_{0}^{L} \mathbf{N}_{w}^{T} q dx = \mathbf{0} \tag{65}$$

which can be expressed in form of standard finite element discrete equations

$$\mathbf{K}_{e} \delta_{e} = \mathbf{F}_{e} \tag{66}$$

where

$$\mathbf{K}_{e} = \int_{0}^{L} \mathbf{N}_{\varepsilon}^{T} \mathbf{D} \mathbf{N}_{\varepsilon} dx + \int_{0}^{L} k_{cs} \mathbf{N}_{cs}^{T} \mathbf{N}_{cs} dx, \quad \mathbf{F}_{e} = \int_{0}^{L} \mathbf{N}_{w}^{T} q dx \tag{67}$$

After assembly of matrices $\mathbf{K}_{e}$ and $\mathbf{F}_{e}$, the global finite element equations can be described as

$$\mathbf{K} \delta = \mathbf{F} \tag{68}$$

where $\mathbf{K}$ and $\mathbf{F}$ are the global stiffness matrix and global load vector.

As it can be seen from Fig. 2(a), the essential boundary conditions of a cantilever can be imposed on Eq. (68), and subsequently solved by the numerical method.

In the structural analyses and design, the internal force analyses of composite beams have been paid much attention, which will also be took into account in the following sections of this paper. The internal forces are defined herein as

$$M_{c} = \iint_{A_{c}} \sigma_{c} y_{c} dA_{c}, \quad M_{s} = \iint_{A_{s}} \sigma_{s} y_{s} dA_{s} \tag{69}$$

$$F_{c} = \iint_{A_{c}} \sigma_{c} dA_{c}, \quad F_{s} = \iint_{A_{s}} \sigma_{s} dA_{s} \tag{70}$$

where M_{c} and M_{s} denote the bending moments of layer c and s, respectively; F_{c} and F_{s} denote the axial forces of layer c and s, respectively.

5. Numerical results and analyses

5.1 Verification

To verify the solutions obtained by the exact and finite element methods in this paper, two examples for comparison have been conducted with the help of solutions of Xu and Wang (2012), Xu and Wu (2007), Schnabl *et al.* (2007b). In their models, each sub-element of the two-layer composite beams was described by Timoshenko or Euler-Bernoulli beam theory.

5.1.1 Numerical example 1
For the sake of comparison, the geometric and material properties herein used are the same as

those of Xu and Wang (2012) (see Fig. 4), where the Young's moduli are E_c=12 GPa and E_s=8 GPa; the Poisson's ratios are ν_c =0.3 and ν_s=0.2 for layer c and s respectively; the stiffness of shear connectors is k_{cs}=50 MPa; the overall length of the beam is L=4 m; the uniformly distributed load is q=1 kN/m. With the aim of examining the reliability of the proposed FEM, we mesh the entire span of cantilever composite beams into three groups: FEM (1), FEM (2) and FEM (3) which are meshed by one, two, or ten even length elements respectively. According to the present exact solving procedure and the aforementioned structural parameters, the exact solution for deflection is obtained in Eq. (71), from which the exact solutions in Table 1 are evaluated. Table 1 apparently shows that the analytical deflections of cantilever composite beams based on the present beam theory are stably larger than those based on the theory of Xu and Wang (2012) who imposed an extra constraint that each sub-element has the same shearing strain, though the Timoshenko kinematics was still applied to each layer of the composite beams. This may be explained by the fact that the extra constraint stiffens the cantilever, as a result, some smaller deflections may be observed. Furthermore, in this table, the rapid convergence of finite element solutions to the exact solutions can be observed as the meshing refines from FEM (1) to (3), which, to some extent, verifies the correctness and reliability of the proposed FE formulation and the program implemented.

$$w(x) = (2.14423 - 2.33642 \times 10^{-4} e^{-211.676x} - 2.73655 \times 10^{-3} e^{-23.0232x} - 2.14120 e^{-2.10162x}$$

$$-5.67984 \times 10^{-5} e^{2.10162x} - 4.61233x - 6.09012x^2 + 1.11111x^3 - 6.94444 \times 10^{-2} x^4) \times 10^{-3} \quad (71)$$

In order to investigate the shear effects, the evolution of the maximum deflection of a cantilever with a variation of beam length from 0.8 m to 4.0 m is shown in Table 2, where Xu and Wu (2007) (TBT), Xu and Wu (2007) (EBT) denote the solutions of Xu and Wu (2007) based on the Timoshenko and Euler-Bernoulli beam theories respectively. Similar to the case of Table 1, the

Table 1 Comparison among numerical results of literature and the present [mm]

References	x [m]			
	1.00	2.00	3.00	4.00
Present exact solutions	7.778804	23.69896	42.16388	60.66850
Present FEM (1)	—	21.30830	—	59.87460
Present FEM (2)	7.402415	23.60789	41.90751	60.49662
Present FEM (3)	7.776838	23.69717	42.16194	60.66666
Xu and Wang (2012)	7.619002	23.54768	42.06997	60.35714

Table 2 Maximum deflection of cantilever with different L/H [mm]

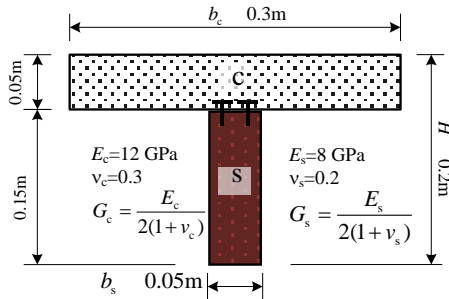| References	L/H			
	20	10	5	4
Present exact solution	60.6685	4.8150	0.4580	0.2173
Present FEM (1)	59.8746	4.7190	0.4512	0.2147
Present FEM (2)	60.4966	4.8025	0.4571	0.2169
Present FEM (3)	60.6666	4.8148	0.4579	0.2172
Xu and Wu (2007) (TBT)	60.5534	4.7876	0.4516	0.2133
Xu and Wu (2007) (EBT)	60.4514	4.7621	0.4452	0.2092

Fig. 4 Geometric parameters used in Xu and Wu (2007), Xu and Wang (2012) and the present
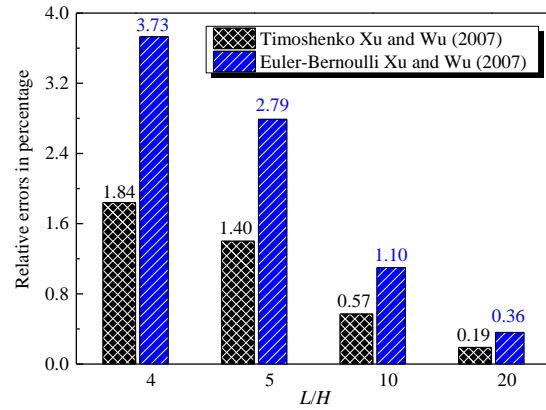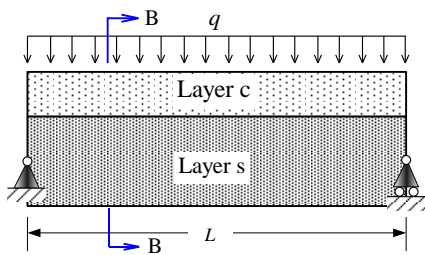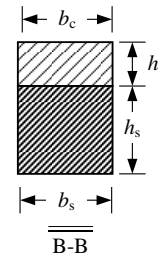

Fig. 5 Relative errors of Xu and Wu (2007) to the present HBT model

(a) A simply supported composite beam profile   (b) Cross section dimensions

Fig. 6 Computational model used in Schnabl *et al.* (2007b) and the present model

deflections computed based on the HBT are again larger than those based on Timoshenko or Euler-Bernoulli beam theories. Further on, Fig. 5 is given to visualize the relative errors of Xu and Wu (2007) to the present higher order composite beams. The relative error of the results based on TBT to those based on HBT is defined as $(w_{HBT}-w_{TBT})/w_{HBT}$ and that for EBT is defined as $(w_{HBT}-w_{EBT})/w_{HBT}$, where w_{HBT}, w_{TBT} and w_{EBT} indicate the deflection resulting from the present HBT, TBT and EBT respectively. It clearly illustrates that shear effects intensify with the decrease of slenderness ratio *L/H*; the errors due to the higher order shear deformation in conjunction with the extra constraint aforementioned are almost half the errors of Euler-Bernoulli beam theory. Moreover, the fact that the solutions of FEM (1), FEM (2) and FEM (3) in Table 2 converge rapidly toward the exact analytical solutions proves the reliability of the proposed FEM again.

5.1.2 Numerical example 2

As is observed in the last section that the extra constraint imposed by Xu and Wu (2007) on the shearing strain may cause an extra error, this numerical example aims to examine the performances of the Timoshenko composite beams without such extra constraint. The results of the present finite element program are compared with those of Schnabl *et al.* (2007b) who had proposed the exact analytical solutions for the problem this paper deals with, based on the TBT without the extra constraint Xu and Wu (2007) imposed.

Fig. 6(a) shows a simply supported composite beam structure with uniform pressure *q*=50

kN/m acting on the top surface of the upper layer. The Young's moduli of layer c and s are both 12 GPa; the shear moduli of layer c and s are both 750 MPa. The cross section, as is shown in Fig. 6 (b), is composed of two rectangles, where they share the same width $b_c=b_s=0.3$ m, and $h_c=0.2$ m, $h_s=0.3$ m; the span of composite beams is $L=5$ m. The proposed FEM is used in this example, and the results are tabulated in Table 3. The relative errors between these models are also visualized in Fig. 7. In order to obtain the reliable FE solutions, there are 100 elements used in the FE model, which can be regarded as a well enough meshing compared with the case of FEM (3) used in the last section. It is suggested by Table 3 and Fig. 7 that the results of models based on TBT and HBT are quite close to each other, which reveals that the constraint of assuming equal shearing strain of layers has a crucial influence on the static mechanical behavior of composite beams. However, a serious relative error of the EBT model is observed, due to the complete neglect of the shear strain throughout each layer. And the errors basically increase with the increase of the interfacial stiffness.

Table 3 Deflection at the mid-span of the two-layer composite beams for different values of interfacial spring stiffness

k_{cs} [MPa]	Present			Schnabl *et al*. 2007b		
	HBT* [mm]	HBT [mm]	EBT* [mm]	EBT [mm]	TBT* [mm]	TBT [mm]
0.01		40.62		38.75		40.62
0.1		40.57		38.69		40.57
1		40.06		38.18		40.05
10	12.56	35.74	10.85	33.91	12.52	35.73
100		21.56		19.82		21.54
500		14.95		13.25		14.94
1000		13.81		12.3		13.79
10000		12.69		10.98		12.67

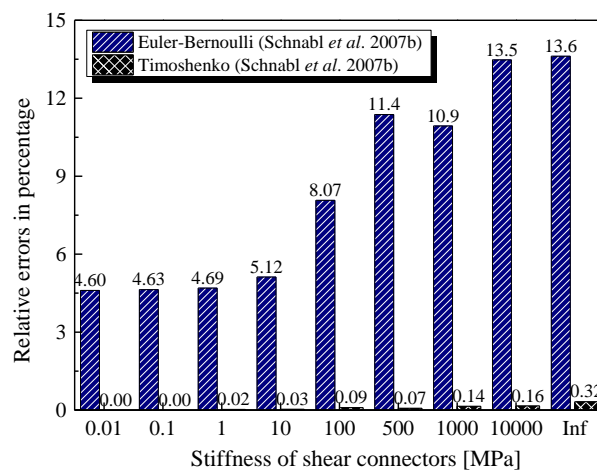Note: columns titled with * denote that the models are with rigid connection between the layers.

Fig. 7 Relative errors of Schnabl *et al*. (2007b) to the present higher order beam theory (herein Inf indicate the case of full composite beams)
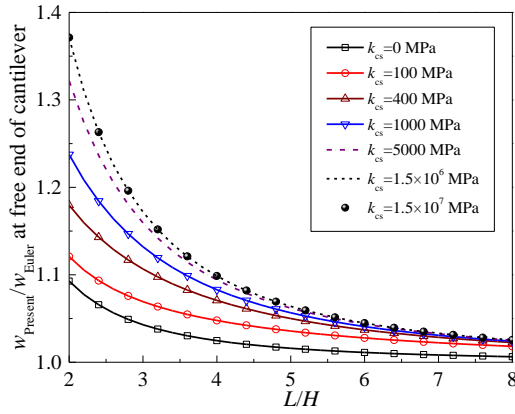
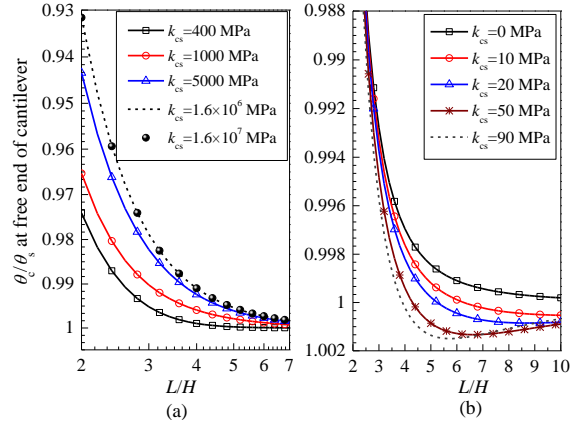Fig. 8 Shear effects on deflection vs *L/H* for different k_{cs}

Fig. 9 Influence of *L/H* on θ_c/θ_s for different k_{cs}

5.2 Parametric study

In this section, the proposed finite element model is used to conduct a parametric study in order to investigate the influence of material and geometric parameters including stiffness of the connectors, span-to-depth ratios and shear modulus factors, on the global structural behavior and stress distribution of the two-layer cantilever discussed in section 5.1.1. Hereafter the basic parameters shown in Fig. 4 are still in use, i.e., the Young's moduli of layer c and s are E_c=12 GPa and E_s=8 GPa, respectively; the shear moduli of layer c and s are G_c=4.6154 GPa and G_s=3.3333 GPa, respectively; the dimensions of the cross section is assigned throughout this section as b_c=0.3 m, b_s=0.05 m, h_c=0.05 m and h_s=0.15 m. The stiffness of the shear connectors is k_{cs}=50 MPa, if the exact value of k_{cs} isn't assigned in the following analyses; the span of the cantilever is determined by the span-to depth ratio *L/H*, which will be stated in the analyses.

The shear effects of the two-layer composite beams have received much attention. As is observed in the Timoshenko composite beams by Schnabl *et al.* (2007a, b), the slenderness ratio *L/H* and the shear connectors' stiffness have a major influence on the shear effects. The main interest of Fig. 8 is also focused on the shear effects due to span-to-depth ratio *L/H* and stiffness of shear connectors k_{cs}, where $w_{Present}$ represents the deflection based on the present HBT; w_{Euler} is approximated by amplifying the shear moduli by 10,000 times. Thus, the ratio of $w_{Present}$ to w_{Euler} indirectly indicates the shear effects on deflection. As it can be seen in Fig. 7, the ratio of $w_{Present}/w_{Euler}$ decreases and approaches to one with the increase of span-to-depth ratio *L/H*, which indicates that the shear effects decrease on the deflection as the composite beams get more slender. Moreover, shear effects are to intensify as the shear connectors become stiffer until it reaches some large value, for example, when k_{cs} approaches to 1.6×10^6 MPa shear effects approach to the maximum.

Fig. 9 is to illustrate the evolution of cross-sectional rotation ratio θ_c/θ_s with the variation of *L/H* for different k_{cs}. It can be seen from both Fig. 9(a) and (b) that θ_c/θ_s converges to 1 as the *L/H* increases, which illustrates that θ_c and θ_s approach to each other when the cantilever get more slender. This also imply that the constraint of assuming $\theta_c=\theta_s$ may not fit well when the beams are deep. Not only the slenderness ratio *L/H* affects the θ_c/θ_s, stiffness of shear connectors k_{cs} also

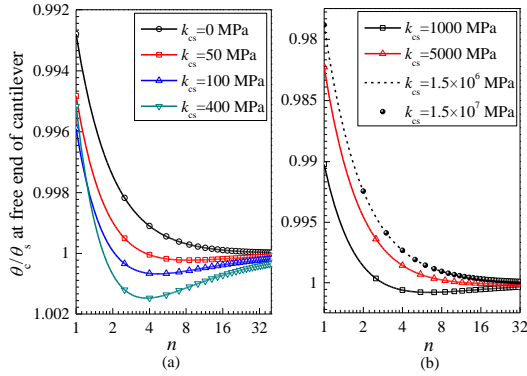Fig. 10 θ_c-to-θ_s ratio vs. *n* for different k_{cs}, with $q = 1$ kN/m and $L/H = 3$
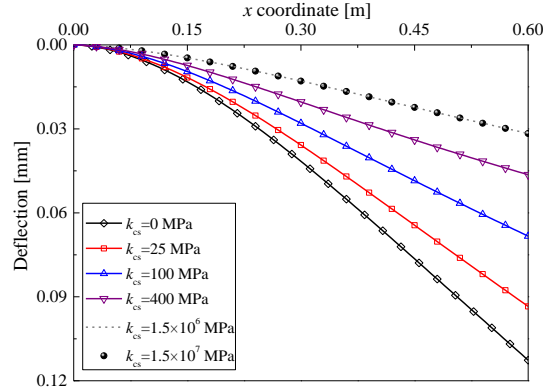

Fig. 11 Influence of stiffness of shear connectors on deflection, with $q = 1$ kN/m and $L/H = 3$
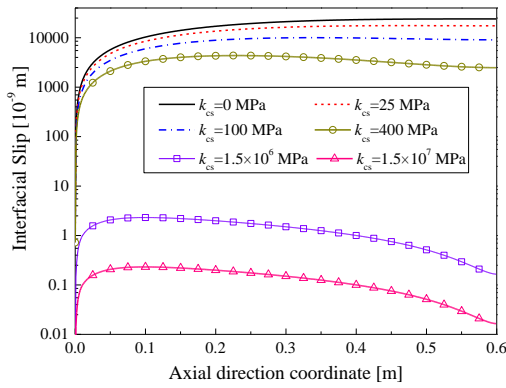

Fig. 12 Influence of stiffness of shear connectors on interfacial slip, with $q=1$ kN/m and $L/H=3$
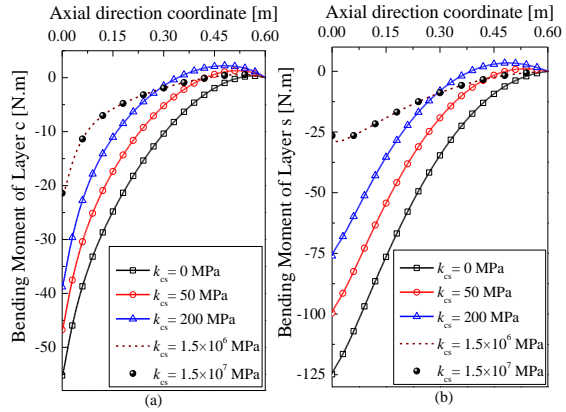

Fig. 13 Influence of stiffness of shear connectors on bending moment of each layer, with $q=1$ kN/m and $L/H=3$

sways the ratio of θ_c/θ_s. Fig. 9(a) and (b) show that the rigidity of shear connectors tends to make θ_c/θ_s increase as the k_{cs} increases when k_{cs} is small (e.g., $k_{cs}<90$ MPa in this example), on the contrary, θ_c/θ_s tends to decrease if k_{cs} is large (e.g., $k_{cs}>400$ MPa in this example).

Fig. 10 (a) and (b) are devoted to studying the influence of shear modulus factor *n* and stiffness of shear connectors on θ_c/θ_s. Herein *n* is defined as $n = \tilde{G}_c / G_c = \tilde{G}_s / G_s$, where $\tilde{G}_c$ and $\tilde{G}_s$ are

shear moduli used in Fig. 10 for layer c and s, respectively; the values of G_c and G_s are shown in Fig. 4. It can be observed that θ_c/θ_s converges to 1 with the increase of *n*, and the stiffness of shear connectors has similar effects to those shown in Fig. 9 (a) and (b). These phenomena again demonstrate that it may not be suitable to assume $\theta_c=\theta_s$, when *n* has small value and shear connectors are rigid.

The effects of shear connectors on the deflections are presented in Fig. 11. As expected, the deflections decrease with an increasing stiffness of connectors k_{cs}. Exactly, when k_{cs} increases from 0 MPa to 1.57×10^7 MPa, the deflections drop by 256% at the free end of the cantilever. Likewise,
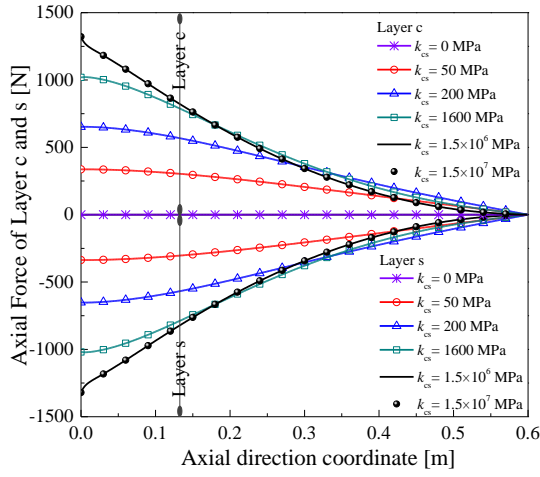
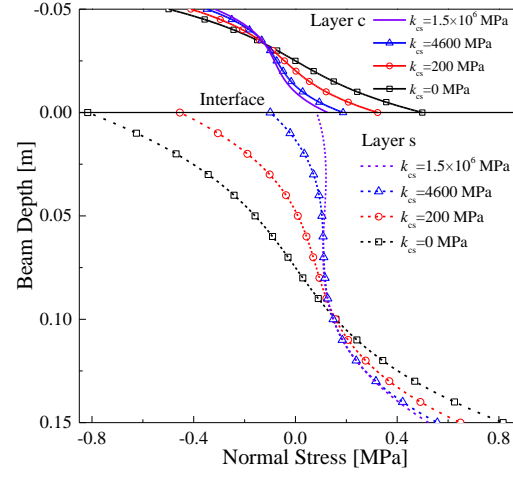Fig. 14 Influence of stiffness of shear connectors on axial force of each layer, with q=1 kN/m and L/H=3

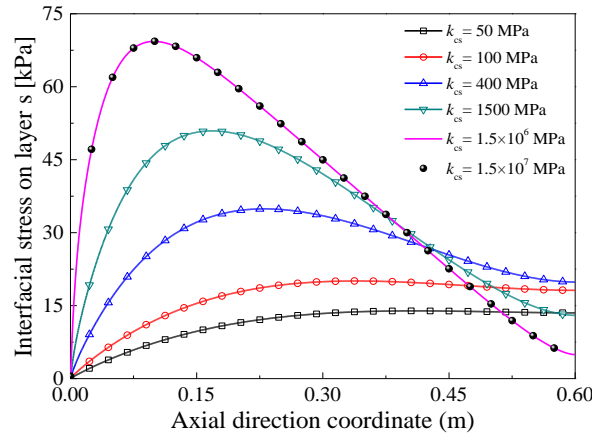Fig. 15 Normal stresses for different k_{cs}, with q=1 kN/m and L/H=3

Fig. 16 Shearing stress along the beam length for different k_{cs}, with q=1 kN/m and L/H=3

Fig. 12 illustrates that the interfacial slip decreases from maximum value to the vicinity of zero as k_{cs} increases from 0 MPa to 1.5×10^7 MPa.

Fig. 13 depicts the distribution of bending moments of each sub-element along the beam axial. It is observed that with the decrease of k_{cs}, bending moment M_c and M_s are increasing at the fixed end of composite beams, until k_{cs} reaches the relative large value 1.5×10^7 MPa. Similarly, Fig. 14 illustrates the distribution of axial force along the x axis. It is suggested that axial force of part c and s are symmetric along the x axis, thus the total axial force of the cross-section is zero, which meets the balance condition of the whole structure. It is noted that the axial force of each sub-element increases with an increasing k_{cs} at fixed end of cantilever as k_{cs} stiffens, until it reaches some large value (e.g., 1.5×10^7 MPa in this case). Moreover, axial force will vanish if k_{cs} drops to zero, which just proves that there is no axial force of single cantilever subjected to the uniform distributed load.

Fig. 15 shows that normal stress over beam depth distributes nonlinearly, unlike the case of beams formulated by traditional EBT or TBT. It should be noted that normal stress based on Euler-Bernoulli or Timoshenko beam theory will distribute linearly over the section, as they conform to planar section hypothesis. In addition, Fig. 15 represents that the normal stress in the vicinity of the interface decreases with the increase of k_{cs}, until k_{cs} achieves some large value, i.e. it approaches to the case of full composite beams. Consequently, it may be inferred that stiff connectors could probably lower the peak normal stress of the whole cross section.

As a supplement to stress analysis, Fig. 16 aims to investigate the interfacial shear stress at the top edge of section s. It is clear to see that the peak shear stresses along the axial direction are increasing as shear connectors get stiffer. As a result, the phenomenon on stress distribution may be utilized in the design of composite beams.

6. Conclusions

In this paper, a new mathematical model for two-layer partial interaction composite beams has been built, where higher order shear deformation of each sub-element is incorporated in the range of linear elastic and small deformation. And the governing differential equations and boundary conditions are formulated according to the principle of minimum potential energy.

The Laplace transform technique is first applied to the static analysis of a cantilever composite beam subjected to uniformly distributed load, and exact solutions are obtained. Besides, the finite element for the analyses is also formulated and implemented. As a result, the solutions of these two methods are in good agreement with each other, which verifies the effectiveness and reliability of the presented methods. More than that, comparison with composite beams based on the classical beam theories is also presented in Tables 1-3, and a brief error analysis has also been carried out in Figs. 5 and 7.

At the end of the paper, the influences of the stiffness of interfacial connectors, span-to-depth ratio and shear modulus factor n, on the deflection, stress distribution and internal force of a composite cantilever are examined using the finite element program implemented. Based on the numerical examples and parametric analyses undertaken, the following main conclusions can be drawn:

• A novel exact analytical method based on the Laplace transform is proposed and verified through the comparisons with the results based on classical beam theories.

• The proposed two-layer composite beam finite element converges at a very high rate to the results from the proposed exact method.

• The slip stiffness and span-to-depth ratio may bring about remarkable shear effects on deflection of cantilever composite beams using the present HBT, especially when L/H is small or k_{cs} is large.

• The assumption of equal shearing strain of each composite layer may not hold well in a case of thick composite beams.

• The nonlinear distribution of normal stresses over the beam depth observed in the composite beams is different from the one based on the traditional beam theories. Peak normal stresses tend to decrease with the increase of k_{cs}, while an increase of the maximum shear stress on top edge of section s along longitudinal direction of cantilever can be achieved with an increasing k_{cs}.

References

Battini, J.M., Nguyen, Q.H. and Hjiaj, M. (2009), "Non-linear finite element analysis of composite beams with interlayer slips", *Comput. Struct.*, **87**(13-14), 904-912.

Čas, B., Saje, M. and Planinc, I. (2004), "Non-linear finite element analysis of composite planar frames with an interlayer slip", *Comput. Struct.*, **82**(23-26), 1901-1912.

Chakrabarti, A., Sheikh, A., Griffith, M. and Oehlers, D. (2012), "Dynamic response of composite beams with partial shear interaction using a higher-order beam theory", *J. Struct. Eng.*, **139**(1), 47-56.

Chakrabarti, A., Sheikh, A.H., Griffith, M. and Oehlers, D.J. (2012), "Analysis of composite beams with longitudinal and transverse partial interactions using higher order beam theory", *Int. J. Mech. Sci.*, **59**(1), 115-125.

Chakrabarti, A., Sheikh, A.H., Griffith, M. and Oehlers, D.J. (2012), "Analysis of composite beams with partial shear interactions using a higher order beam theory", *Eng. Struct.*, **36**, 283-291.

Cook, R.D., Malkus, D.S., Plsha, M.E. and Witt, R.J. (2007), *Concepts and applications of finite element analysis*, John Wiley & Sons.

Dall'Asta, A. and Zona, A. (2002), "Non-linear analysis of composite beams by a displacement approach", *Comput. Struct.*, **80**(27-30), 2217-2228.

Erkmen, R.E. and Attard, M.M. (2011), "Displacement-based finite element formulations for material-nonlinear analysis of composite beams and treatment of locking behaviour", *Finite Elem. Anal. Des.*, **47**(12), 1293-1305.

Faella, C., Martinelli, E. and Nigro, E. (2002), "Steel and concrete composite beams with flexible shear connection: "exact" analytical expression of the stiffness matrix and applications", *Comput. Struct.*, **80**(11), 1001-1009.

Grognec, P.L., Nguyen, Q.H. and Hjiaj, M. (2012), "Exact buckling solution for two-layer Timoshenko beams with interlayer slip", *Int. J. Solid. Struct.*, **49**(1), 143-150.

Hjiaj, M., Battini, J.M. and Huy Nguyen, Q. (2012), "Large displacement analysis of shear deformable composite beams with interlayer slips", *Int. J. Nonlin. Mech.*, **47**(8), 895-904.

Kroflič, A., Planinc, I., Saje, M., Turk, G. and Čas, B. (2010), "Non-linear analysis of two-layer timber beams considering interlayer slip and uplift", *Eng. Struct.*, **32**(6), 1617-1630.

Kroflič, A., Saje, M. and Planinc, I. (2011), "Non-linear analysis of two-layer beams with interlayer slip and uplift", *Comput. Struct.*, **89**(23-24), 2414-2424.

Li, J., Shi, C., Kong, X., Li, X. and Wu, W. (2013), "Free vibration of axially loaded composite beams with general boundary conditions using hyperbolic shear deformation theory", *Compos. Struct.*, **97**(0), 1-14.

Newmark, N., Siess, C. and Viest, I. (1951), "Tests and analysis of composite beams with incomplete interaction", *Proc. Soc. Exp. Stress Anal.*, **9**(1), 75-92.

Nguyen, Q.H., Martinelli, E. and Hjiaj, M. (2011), "Derivation of the exact stiffness matrix for a two-layer Timoshenko beam element with partial interaction", *Eng. Struct.*, **33**(2), 298-307.

Ouyang, Y., Liu, H. and Yang, X. (2012), "Bending of composite beam considering effect of adhesive layer slip", *E. M.*, **29**(9), 215-222.

Ranzi, G., Dall'Asta, A., Ragni, L. and Zona, A. (2010), "A geometric nonlinear model for composite beams with partial interaction", *Eng. Struct.*, **32**(5), 1384-1396.

Ranzi, G. and Zona, A. (2007), "A steel-concrete composite beam model with partial interaction including the shear deformability of the steel component", *Eng. Struct.*, **29**(11), 3026-3041.

Reddy, J.N. (1984), "A simple higher-order theory for laminated composite plates", *J. Appl. Mech.*, **51**(4), 745-752.

Schnabl, S., Saje, M., Turk, G. and Planinc, I. (2007a), "Locking-free two-layer Timoshenko beam element with interlayer slip", *Finite Elem. Anal. Des.*, **43**(9), 705-714.

Schnabl, S., Saje, M., Turk, G. and Planinc, I. (2007b), "Analytical solution of two-Layer beam taking into account interlayer slip and shear deformation", *J. Struct. Eng.*, ASCE, **133**, 886-894.

Vo, T.P. and Thai, H.T. (2012), "Static behavior of composite beams using various refined shear deformation

theories", *Compos. Struct.*, **94**(8), 2513-2522.

Whitney, J. (1973), "Shear correction factors for orthotropic laminates under static load", *J. Appl. Mech. Tran.*, ASME, **40**(1), 302-304.

Xu, R. and Wang, G. (2012), "Variational principle of partial-interaction composite beams using Timoshenko's beam theory", *Int. J. Mech. Sci.*, **60**(1), 72-83.

Xu, R. and Wu, Y. (2007), "Static, dynamic, and buckling analysis of partial interaction composite members using Timoshenko's beam theory", *Int. J. Mech. Sci.*, **49**(10), 1139-1155.

Yang, X. and He, G. (2014), "General analytical method for composite beams' bending using Reddy's higher order beam theory", *C. J. S. M.*, **35**(2), 199-208.

Zona, A. and Ranzi, G. (2011), "Finite element models for nonlinear analysis of steel-concrete composite beams with partial interaction in combined bending and shear", *Finite Elem. Anal. Des.*, **47**(2), 98-118.

CC